ACS APPLIED MATERIALS & INTERFACES

Research Article

www.acsami.org

From Dispersed Microspheres to Interconnected Nanospheres: Carbon-Sandwiched Monolayered MoS_2 as High-Performance Anode of Li-Ion Batteries

Jie Shao,[†] Qunting Qu,*[,†,‡] Zhongming Wan,[‡] Tian Gao,[‡] Zhichen Zuo,[§] and Honghe Zheng*[,‡]

[†]College of Chemistry, Chemical Engineering and Material Science & Collaborative Innovation Center of Suzhou Nano Science and Technology and [‡]College of Physics, Optoelectronics and Energy, Soochow University, Suzhou, Jiangsu 215006, China

[§]Suzhou Power Capacitor Co., LTD, Suzhou, Jiangsu 215122, China

ABSTRACT: Hierarchical structured carbon@MoS_2 (C@MoS_2) microspheres and nanospheres composed of carbon-sandwiched monolayered MoS_2 building blocks are synthesized through a facile one-pot polyvinylpyrrolidone (PVP) micelle-assisted hydrothermal route. The dimension and carbon content of C@MoS_2 spheres are effectively controlled by singly adjusting the concentration of PVP, which plays the dual functions of soft-template and carbon source. As the anode materials of Li-ion batteries, C@MoS_2 nanospheres present considerably higher capacity, better rate behavior and cycling stability than C@MoS_2 microspheres. The reasons are attributed to the unique interconnected nanospherical morphology and the internal hierarchical construction of C@MoS_2 nanospheres with expanded MoS_2/carbon interlayer spacing.

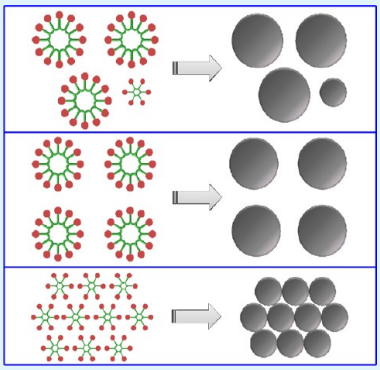

KEYWORDS: *carbon, composites, Li-ion batteries, molybdenum disulfide, nanospheres*

1. INTRODUCTION

MoS_2 as a representative two-dimensional (2D) layered material has attracted considerable attention in energy storage and conversion systems especially in Li-ion batteries (LIBs). The weak van der Waals interaction between MoS_2 layers favors intercalation/extraction of various cations, and meanwhile the four-electron conversion reaction of MoS_2 upon cations uptake brings about a significantly higher capacity than the intercalation reaction-based graphite anode.[1−7] Nevertheless, MoS_2 suffers from poor rate behavior and rapid capacity fading resulting from its low electrical conductivity and substantial volume change during charge/discharge.

To address these issues, significant efforts have been devoted to fabricating MoS_2/carbon nanocomposites of special construction since carbon can play the dual roles of enhancing electron transport and improving structural stability of electrode.[1−4,8−12] Various carbon materials, such as carbon nanotubes or nanofibers,[2,13,14] graphene nanosheets or networks,[15−21] carbon spheres,[22] and porous carbon,[23] have been combined with 2D MoS_2 to enhance the capacity, rate capability, and cycle life of batteries. Very recently, a novel MoS_2/carbon hybrid nanoarchitecture consisting of alternately stacked single-layer MoS_2 and carbon was reported to possess the ideal atomic interface contact, which could maximize the synergistic effect of MoS_2 and carbon for Li^+ storage.[24] However, preparation of this ideal MoS_2/carbon construction involves a multistep procedure, namely, preformation and treatment of monolayered MoS_2, coating of carbon precursor, and subsequent annealing. In this regard, it is appealing to explore a simpler approach to synthesize MoS_2/carbon hybrid with such kind of ideal interface contact.

Besides, fabrication of hierarchical MoS_2 microarchitectures has aroused great interest because the 2D MoS_2 building blocks can provide highly exposed active edge sites, while the primary microarchitecture can prevent aggregation and pulverization of MoS_2 layers during charge/discharge cycles.[3,25−30] In our previous work, we reported the synthesis of hierarchical quasi-hollow MoS_2 microspheres with an average size of 600 nm using monodisperse sulfonated polystyrene microspheres as template.[25] Ultrathin MoS_2 nanosheets supported on N-doped carbon boxes with dimension of ∼600 nm were prepared by Lou and co-workers[3] using Fe_2O_3 cubes as sacrificial template. $MnCO_3$ microcubes were also used as the template to synthesize hollow MoS_2 microboxes with uniform size of ∼3 μm.[31] These results demonstrate the successful syntheses of hierarchical MoS_2 microarchitectures with submicron or micrometer-scaled dimension, whereas synthesis of hierarchical MoS_2 nanoarchitecture with size of less than 100 nm remains a great challenge.

In this work, we present the controllable syntheses of hierarchical carbon@MoS_2 (C@MoS_2) spheres from submicron to nanoscaled size through a one-pot polyvinylpyrrolidone (PVP) micelle-assisted hydrothermal route. The morphology and carbon content of C@MoS_2 spheres are effectively

Received: July 4, 2015
Accepted: October 1, 2015
Published: October 1, 2015

DOI: 10.1021/acsami.5b06002
ACS Appl. Mater. Interfaces 2015, 7, 22927−22934

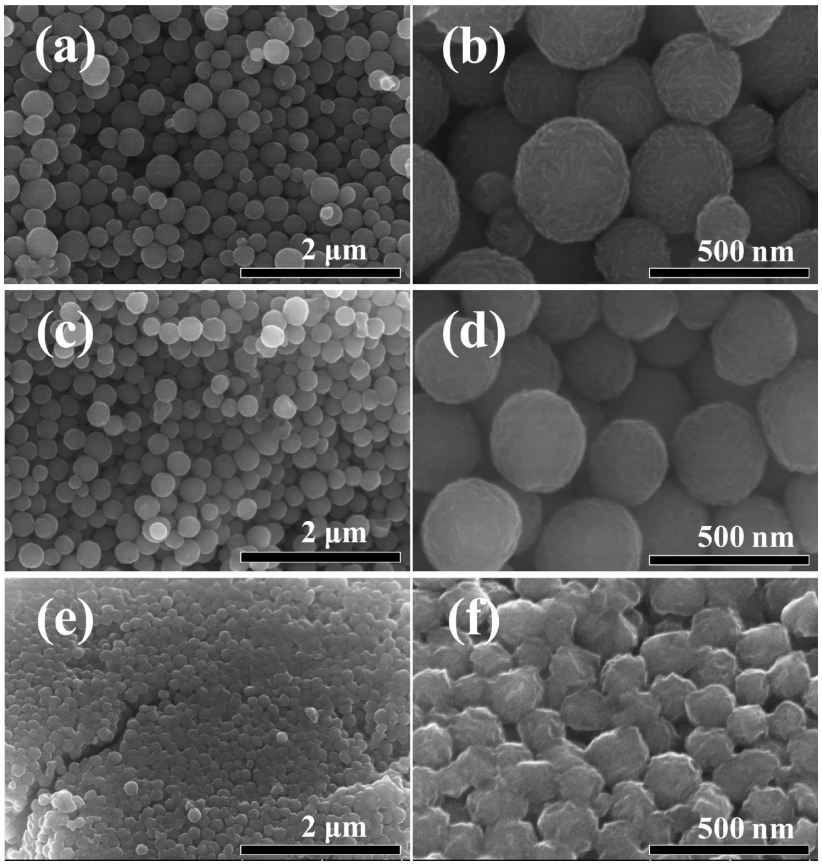

Figure 1. SEM images of (a, b) 0.2-C@MoS_2, (c, d) 0.4-C@MoS_2, and (e, f) 0.8-C@MoS_2.

controlled by singly adjusting the concentration of PVP, which plays the dual functions of soft-template and carbon source. More importantly, the C@MoS_2 nanospheres are composed of loosely and alternately stacked MoS_2 and carbon monolayers, endowing this material with high capacity, good structural stability, and high-rate behavior as anode material of Li-ion batteries.

2. EXPERIMENTAL PROCEDURES

2.1. Synthesis of C@MoS_2 Composites. A certain amount of PVP (K30, molecular weight 40 000) was first dissolved in 40 mL of distilled water by stirring at room temperature for 1 h. Next, 0.48 g of Na_2MoO_4 and 0.96 g of thiourea were added into the PVP solution. After it was stirred for 1 h, the mixture solution was transferred into a 50 mL Teflon-lined stainless steel autoclave and heated at 200 °C for 24 h. The precipitates were collected through centrifuge, washed with water, and then dried at 60 °C. At last, the intermediates were annealed at 800 °C for 2 h under Ar atmosphere to carbonize PVP and improve the crystallinity of MoS_2. The C@MoS_2 composites obtained with addition of 0.2, 0.4, and 0.8 g of PVP are denoted as 0.2-C@MoS_2, 0.4-C@MoS_2, and 0.8-C@MoS_2, respectively. Bulk MoS_2 was prepared through the same procedure but without the addition of PVP.

2.2. Characterization Methods. Scanning electron microscopy (SEM) images were obtained using Hitachi S-8010 equipment operated at 15 kV. X-ray diffraction (XRD) patterns were collected using PANalytical X'Pert PRO MRD diffractometer with Ni-filtered Cu Kα radiation. Thermogravimetric (TG) analysis was performed using a SEIKO TG/DTA 7300 thermal analyzer. Field-emission Raman spectra were measured through JobinYvon LabRAM HR800 Raman spectrometer with an excitation wavelength of 514 nm. Transmission electron microscopy (TEM) images were obtained using FEI Tecnai G-20 microscope. Elemental mapping was achieved using the affiliated energy dispersive X-ray (EDX) spectrometer of Hitachi S-8010 equipment.

2.3. Electrochemical Testing. The electrode slurries were prepared by homogeneously dispersing C@MoS_2 active materials, Super P−Li, and poly(vinylidene fluoride) with a weight ratio of 8/1/1 in *N*-methylpyrrolidone. The slurry was spread onto copper foil and then dried in an oven at 80 °C for 1 h. Next, the copper foil was cut into small disks with uniform diameter of 13 mm. The mass loading of C@MoS_2 active material on each copper disk is ~2 mg. The electrode disks were further dried in a vacuum over at 120 °C overnight to assemble the CR2032 coin cells. Lithium foil was used as the counter electrode. 1.0 M $LiPF_6$ dissolved in ethyl carbonate/dimethyl carbonate (1:1 v/v ratio) and Celgard 2500 were used as the electrolyte and separator, respectively. Galvanostatic discharge and charge tests were performed with a cycle tester from LAND Electronic Co. The cutoff potential window was set between 3.0 and 0.01 V.

3. RESULTS AND DISCUSSION

The precursor solutions containing the same amounts of Na_2MoO_4 and thiourea but with different amounts of PVP were used for the syntheses of different C@MoS_2 samples. PVP functioning as the soft-template and carbon source influences not only the morphology but also the carbon content of C@MoS_2. With the increase of PVP content (0.2, 0.4, and 0.8 g), the three products are denoted as 0.2-C@MoS_2, 0.4-C@MoS_2, and 0.8-C@MoS_2, respectively. To help description, the submicron-scaled spheres with size of considerably larger than 100 nm are called microspheres. SEM was used to investigate the morphologies of these materials. SEM images of 0.2-C@MoS_2 (Figure 1a,b) show that it is composed of uniform spherical particles. Most of the microspheres have a diameter ranging from 250 to 350 nm, and a small amount of

DOI: 10.1021/acsami.5b06002
ACS Appl. Mater. Interfaces 2015, 7, 22927−22934

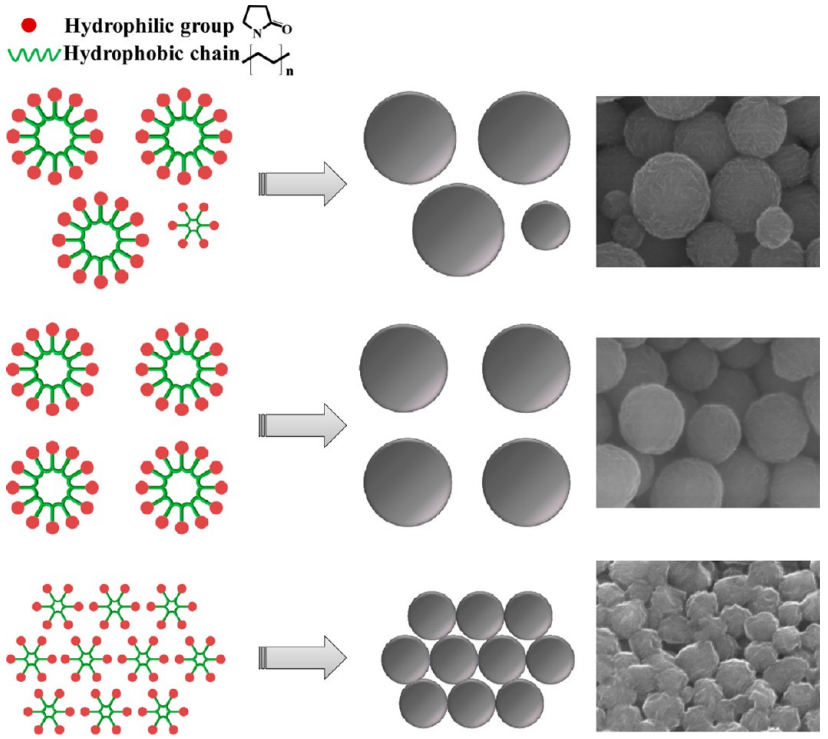

Figure 2. Schematic illustration of the formation of different C@MoS_2 products with morphologies depending on the self-assembly manners of PVP micelles.

nanospheres with size of ~100 nm are also observed clearly. Besides, the surface of these microspheres manifests distinct nanoflakes-like morphology, signifying the existence of hierarchical structure. Actually, nanoflakes or nanosheets-like MoS_2 is generally obtained due to its inherent 2D crystalline structure.[2,3,31] Compared to 0.2-C@MoS_2, the dimension of 0.4-C@MoS_2 microspheres is more homogeneous exhibiting an average diameter of ~250 nm, whereas small nanospheres are seldom observed in this composite (Figure 1c,d). Moreover, the nanoflakes-like surface of these microspheres becomes less distinguishable due to the incorporation of more PVP-derived carbon into the composite. For the 0.8-C@MoS_2 (Figure 1e,f), diameter of these spheres drastically decreases to the nanoscaled size of ~100 nm. More interestingly, these nanospheres are interconnected with each other, in sharp contrast to those dispersed microspheres of 0.2-C@MoS_2 and 0.4-C@MoS_2.

Formation of these C@MoS_2 products with morphologies depending on the concentrations of PVP is schematically illustrated in Figure 2. It has been well-researched that PVP as a hydrosoluble surfactant can self-assemble into spherical vesicular micelles in water with their hydrophilic amide groups pointed outward and hydrophobic alkyl backbones pointed toward the interior.[32] These micelles are capable of functioning as the soft-template to direct the formation of materials with special spherical morphology. Various materials such as polystyrene, Fe-based zeolitic imidazolate framework, and sulfur particles have been successfully fabricated into microspherical structures with the assistance of PVP.[33−35] By analogy, MoS_2 microspheres with the shape and dimension directly dependent on the self-assembly manners of PVP micelles also can be fabricated. On the basis of the SEM images of C@MoS_2 samples, it is reasonable to assume that, at a low PVP concentration (0.2 g PVP), dispersed micelles, with the majority of them belonging to submicron-scaled size and the minority of them possessing nanoscaled size, should be formed. As a result, large amounts of C@MoS_2 microspheres combined with small amounts of C@MoS_2 nanospheres are obtained. As the PVP content increases to 0.4 g, the dimension of microspherical PVP micelles becomes more homogeneous, resulting in the formation of homogeneous 0.4-C@MoS_2 microspheres. At a high PVP concentration (0.8 g PVP), PVP could assemble into interconnected nanoscaled micelles to realize its stable dispersion in water. Consequently, interconnected nanospheres are obtained for 0.8-C@MoS_2.

The Li^+ storage performances of C@MoS_2 samples were investigated using Li foil as the counter electrode. Cyclic voltammetry (CV) is an effective and common technique for investigating the electrochemical reaction of electrode materials. The initial three CV curves of C@MoS_2 electrodes at a scan rate of 0.1 mV s^{-1} are shown in Figure 3a−c. During the first negative scan, two cathodic peaks at ~0.7 and 0.5 V are observed distinctly for 0.2-C@MoS_2 and 0.4-C@MoS_2. The first peak at 0.7 V can be attributed to the phase transformation of MoS_2 upon Li^+ intercalation into MoS_2 lattice to form Li_xMoS_2.[36,37] The second peak at ~0.5 V results from the conversion reaction accompanied by the formation of metal Mo embedded in Li_2S.[18] Compared to 0.2-C@MoS_2 and 0.4-C@MoS_2, one significant feature of 0.8-C@MoS_2 during the first negative scan is that the cathodic peak at ~0.7 V corresponding to Li^+ intercalation is inconspicuous, while the peak at 0.5 V representative of the conversion reaction is strong. The peculiar electrochemical reaction of 0.8-C@MoS_2 during the first negative scan is believed to result from its unique crystalline structure, which will be validated from the following materials characterization. During the subsequent positive scan, delithiation of Li_2S accompanied by the formation of sulfur gives rise to a pronounced anodic peak at ~2.3 V.[36] During the second and

DOI: 10.1021/acsami.5b06002
ACS Appl. Mater. Interfaces 2015, 7, 22927−22934

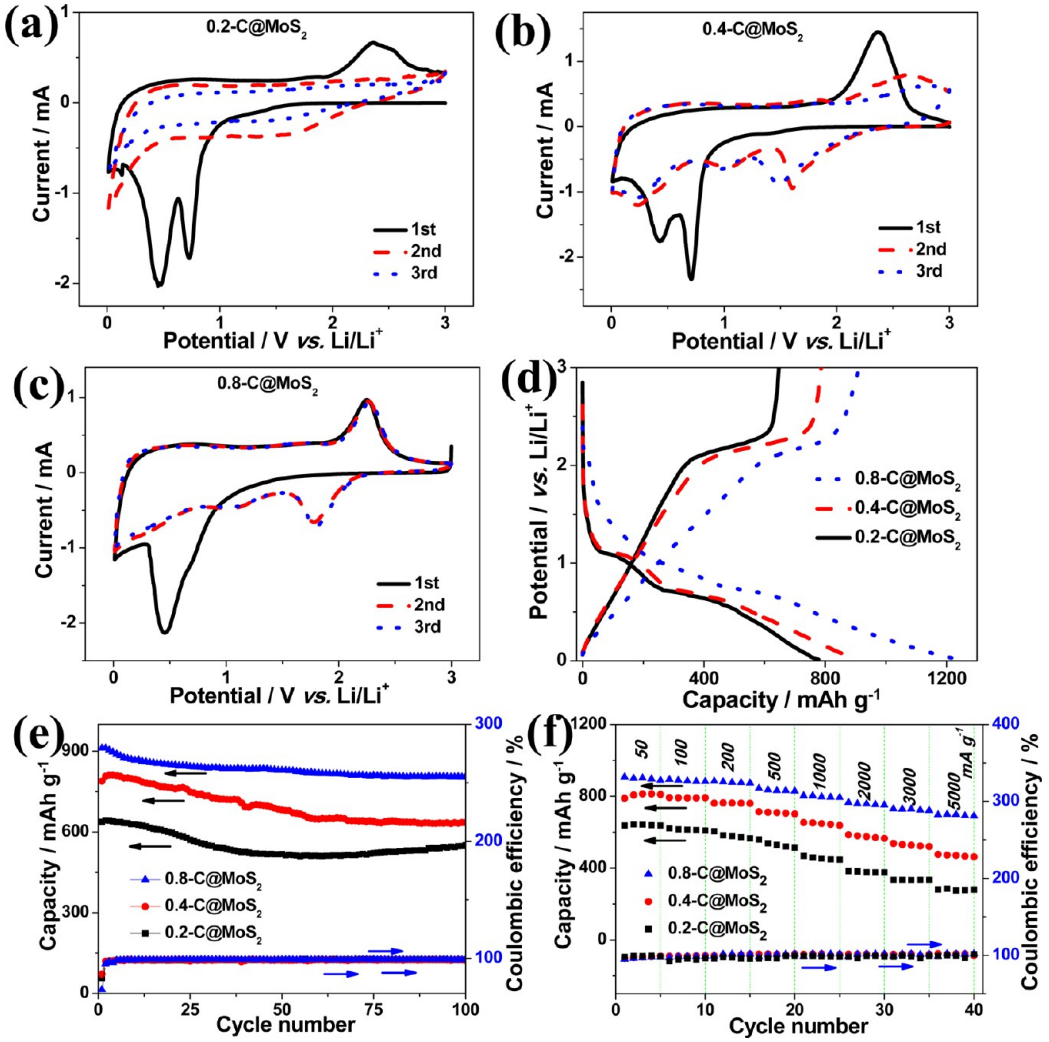

Figure 3. (a–c) CV curves at a scan rate of 0.1 mV s^{-1}, (d) the initial discharge/charge curves, (e) cycling performance, and (f) rate behaviors of the three C@MoS_2 electrodes.

third negative scans, the significant current response occurs at ~1.8 V, corresponding to the conversion reaction of sulfur to Li_2S. In addition, it is notable that the intensities of the anodic peaks of 0.2-C@MoS_2 and 0.4-C@MoS_2 decrease drastically in the second and third scans. In contrast, the anodic peaks of 0.8-C@MoS_2 perfectly overlap during the initial three scans, suggesting its excellent electrochemical reversibility and stability.

The initial galvanostatic discharge/charge curves of the three electrodes at a current density of 100 mA g^{-1} are compared in Figure 3d. For the 0.2-C@MoS_2 and 0.4-C@MoS_2 electrodes, two potential plateaus at ~1.1 and 0.6 V are observed during discharge due to the Li^+ intercalation reaction followed by a conversion reaction. In contrast, the 0.8-C@MoS_2 electrode presents only one potential plateau at ~0.6 V, whereas the plateau corresponding to Li^+ intercalation disappears. During the subsequent charge of the three electrodes, the distinct plateaus at 2.3 V are attributed to the delithiation of Li_2S to form sulfur. The information reflected by these discharge/charge curves are in good agreement with that of CV curves. The reversible (charge) capacities of 0.2-C@MoS_2, 0.4-C@MoS_2, and 0.8-C@MoS_2 in the first cycle are 646, 786, and 911 mAh g^{-1}, respectively, meaning that 0.8-C@MoS_2 nanospheres exhibit the highest utilization efficiency of active material.

The reversible capacity evolutions of the three electrodes at various current densities are shown in Figure 3e. Obviously, 0.8-C@MoS_2 nanospheres exhibit significantly better rate behavior than 0.4-C@MoS_2 and 0.2-C@MoS_2 microspheres. When the current density rises to 5000 mA g^{-1}, 0.8-C@MoS_2 retains 690 mAh g^{-1} of capacity, which is considerably better than that of quasi-hollow MoS_2 microspheres (560 mAh g^{-1} at 5000 mA g^{-1})[25] and N-doped carbon@MoS_2 boxes (531 mAh g^{-1} at 4000 mA g^{-1}).[3] The long-term cycling performance of these C@MoS_2 composites was evaluated through repetitive discharge/charge at a constant current density of 100 mA g^{-1} (Figure 3f). After 100 continuous cycles, the reversible capacities of 0.2-C@MoS_2, 0.4-C@MoS_2, and 0.8-C@MoS_2 maintain at 549, 639, and 807 mAh g^{-1}, respectively, suggesting the superior structural stability of 0.8-C@MoS_2.

Apparently, the superior Li^+ storage performance of 0.8-C@MoS_2 as compared to 0.2-C@MoS_2 and 0.4-C@MoS_2 can be easily correlated with its unique interconnected nanospherical construction as disclosed by SEM images. The interconnected spherical structure can facilitate the transport of electrons/Li-ions through the whole electrode, while the nanoscaled spheres can shorten the diffusion length of Li ions. To find the reasons for the peculiar electrochemical reaction of 0.8-C@MoS_2 during the first cycle and elucidate other possible reasons

DOI: 10.1021/acsami.5b06002
ACS Appl. Mater. Interfaces 2015, 7, 22927–22934

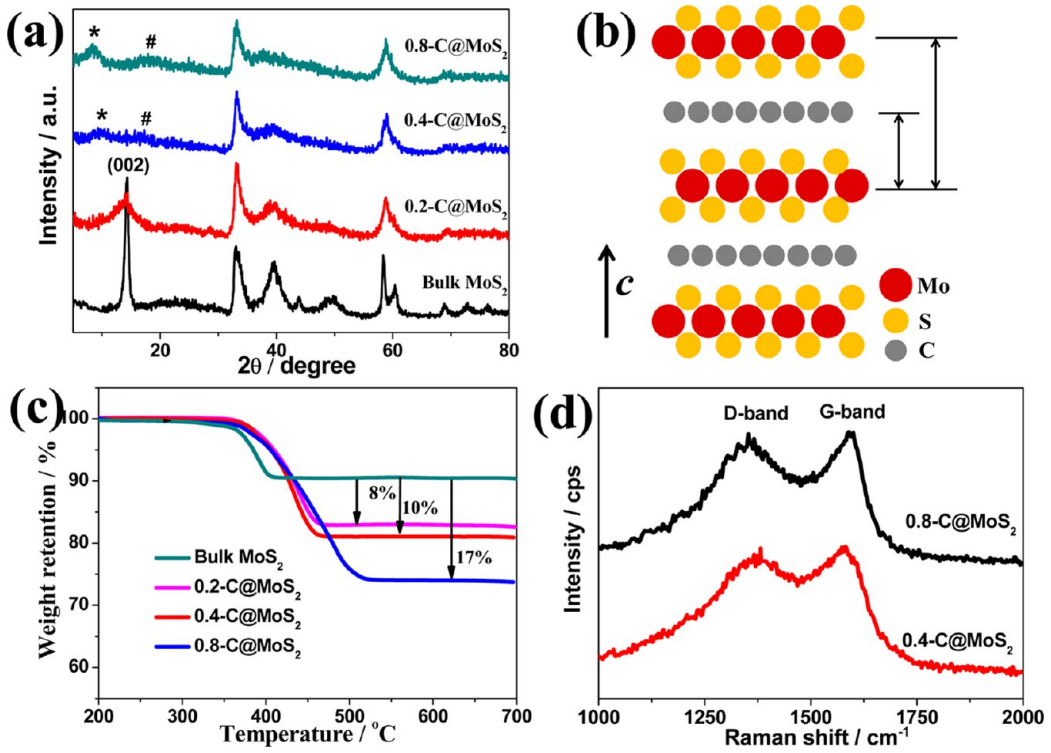

Figure 4. (a) XRD patterns of C@MoS_2 composites and bulk MoS_2. (b) Schematic illustration of the carbon inserted single-layer MoS_2 microstructure along the direction of *c*-axis. (c) TG curves of C@MoS_2 composites and bulk MoS_2. (d) Raman spectra of C@MoS_2 composites.

leading to the different Li^+ storage performance of as-prepared C@MoS_2 composites, the crystalline structure, chemical composition, and hierarchical construction of these C@MoS_2 micro/nanospheres were further investigated in detail.

The crystalline structures of these samples were studied through XRD. As shown in Figure 4a, XRD pattern of 0.2-C@MoS_2 is consistent with that of bulk MoS_2, signifying the successful synthesis of hexagonal MoS_2 phase (JCPDS card No. 37−1492). Especially, the distinct peak at 14.2° characteristic of the (002) crystalline plane of MoS_2 suggests the ordered stacking of S−Mo−S layers. However, the characteristic peak at 14.2° disappears for 0.4-C@MoS_2 and 0.8-C@MoS_2. Meanwhile, two new peaks as marked by asterisk and octothorpe are observed, the diffraction angles of which are similar to those of carbon inserted single-layer MoS_2 nanosheets.[16,24,38] The two new peaks of 0.8-C@MoS_2 are located at 8.6° and 17.8°. According to Bragg's equation, the corresponding interlayer spacing is calculated to be 1.03 and 0.50 nm, respectively. Taking the crystallographic thickness of single-layer MoS_2 and carbon in their 2D layered structures (0.62 and 0.34 nm) into account, a basal spacing of ∼0.96 nm (0.62 + 0.34 nm) will be expected for an ideal carbon inserted MoS_2 hierarchical architecture. Thus, the interlayer spacing of 1.03 nm is close to yet slightly larger than the predicted value of 0.96 nm, suggesting a carbon-inserted MoS_2 structure with expanded interlayer spacing. The interlayer spacing of 0.50 nm can be attributed to the distance between carbon layer and MoS_2 layer as shown in Figure 4b.[16,39] In the case of 0.4-C@MoS_2, one of the new peaks appears at 9.6°, whose interlayer spacing is calculated to be 0.92 nm, slightly narrower than that of 0.8-C@MoS_2. Moreover, the other new peak representing the ordered stacking of carbon and MoS_2 layers is very weak. These phenomena probably result from the low carbon content of 0.4-C@MoS_2 as confirmed by the following TG analysis. The low carbon content is not sufficient to construct a perfectly ordered carbon-inserted MoS_2 structure. Therefore, it is proposed that the distinct carbon-sandwiched MoS_2 structure of 0.8-C@MoS_2 should be the main reason for its unique CV behavior during the first negative scan. The presence of carbon interlayers between the neighboring MoS_2 layers prevents the phase transformation of MoS_2 from trigonal prismatic to octahedral structure upon Li^+ insertion. So the typical cathodic peak of MoS_2 at ∼0.7 V corresponding to intercalation reaction of Li^+ almost disappears in the CV curve of 0.8-C@MoS_2.

The exact carbon contents of the as-synthesized C@MoS_2 composites were determined through TG analysis (Figure 4c). Bulk MoS_2 undergoes a weight loss of 9% at ∼350 °C owing to the oxidative reaction of MoS_2 to MoO_3 under air atmosphere. By comparing the weight losses of bulk MoS_2 and C@MoS_2, the carbon contents in 0.2-C@MoS_2, 0.4-C@MoS_2, and 0.8-C@MoS_2 are determined to be 8%, 10%, and 17%, respectively. It can be seen that the carbon contents are effectively controlled through adjusting the PVP concentration. The highest carbon content of 0.8-C@MoS_2 is capable of providing enough carbon layers to construct the distinct carbon-inserted MoS_2 structure. As a result, the conductive carbon sandwiched between the single-layer MoS_2 can facilitate the transport of electrons, increasing the utilization efficiency of MoS_2 active material, and improving the Li^+ storage capability.

Raman spectroscopy was used to evaluate the quality of carbon since it is another factor affecting the electrical conductivity of C@MoS_2 composite. As shown by the Raman spectra (Figure 4d), both 0.8-C@MoS_2 and 0.4-C@MoS_2 exhibit two obvious peaks at ∼1370 and 1590 cm^{-1}, corresponding to the disordered carbon (D-bond) and ordered graphitic carbon (G-bond), respectively. The relative intensity ratios of the two peaks (I_D/I_G) in 0.8-C@MoS_2 and 0.4-C@MoS_2 are 0.84 and 0.85, respectively, revealing a similar

DOI: 10.1021/acsami.5b06002
ACS Appl. Mater. Interfaces 2015, 7, 22927−22934

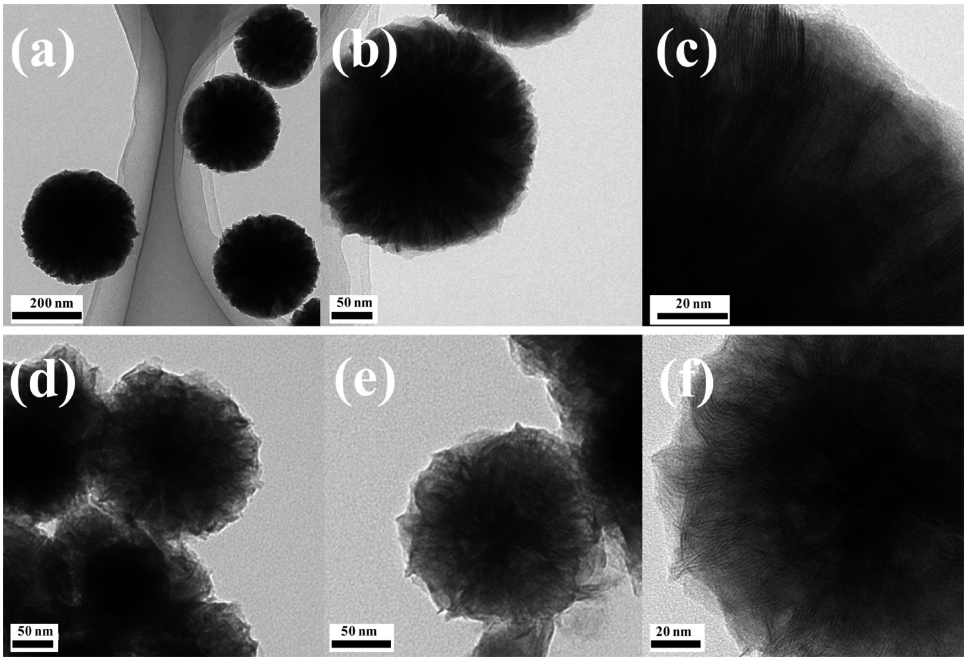

Figure 5. TEM images of (a–c) 0.4-C@MoS_2 microspheres and (d–f) 0.8-C@MoS_2 nanospheres at different magnification.

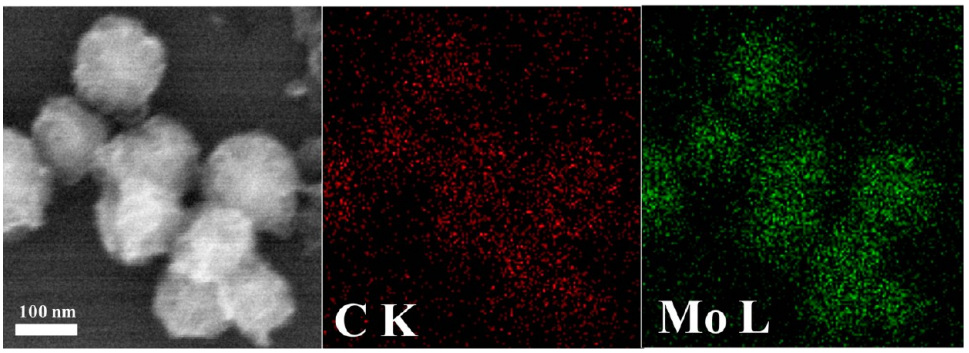

Figure 6. EDX elemental mapping of 0.8-C@MoS_2 nanospheres.

graphitic degree of carbon in the two materials. The I_D/I_G ratios also reflect a high graphitic degree of carbon layers intercalated between the adjacent single-layer MoS_2, which is beneficial for the improvement of electrical conductivity.

We further investigated the hierarchical structures of C@MoS_2 composites through TEM. TEM images of 0.4-C@MoS_2 (Figure 5a–c) show that these microspheres are separated from each other. In these microspheres, the well-defined 2D MoS_2 layers are densely stacked, leading to an extremely dense interior. TEM images of 0.8-C@MoS_2 (Figure 5d–f) show that the obtained nanospheres are interconnected with each other. The interior of these nanospheres seems to be much looser as compared to that of 0.4-C@MoS_2, which can be attributed to the higher carbon content, the decreased number of stacked 2D MoS_2 layers, as well as the wider interlayer distance of carbon inserted MoS_2 layers. Distribution of carbon in 0.8-C@MoS_2 was analyzed through EDX elemental mapping. As shown in Figure 6, C is dispersed uniformly throughout the C@MoS_2 composites.

On the basis of the above characterizations, it is reasonable to assume that the apparent interconnected nanospherical morphology along with the internal hierarchical construction of 0.8-C@MoS_2 contribute to its superior Li^+ storage performance. First, the interconnected nanospheres could accelerate the transport of electrons and Li ions through the whole electrode and shorten the diffusion length of Li ions. Second, the loosely stacked MoS_2/carbon layers with expanded interlayer spacing facilitate transport of Li^+ ions through the basal planes. Third, a large amount of conductive carbon sandwiched between the neighboring single-layer MoS_2 can increase the charge transfer efficiency especially along *c*-direction. Lastly, the incorporation of carbon interlayers can avoid restacking and agglomeration of single-layer MoS_2 during repeated discharge/charge cycling. All these factors contribute to the high capacity, good rate behavior, and cycling stability of hierarchical 0.8-C@MoS_2 nanospheres.

4. CONCLUSION

A facile one-pot approach is presented to synthesize hierarchical C@MoS_2 spheres with controllable submicron or nanoscaled dimension. Remarkably, the as-prepared C@MoS_2 nanospheres are composed of alternately stacked MoS_2 and carbon monolayers. As the anode materials of Li-ion batteries, C@MoS_2 nanospheres present considerably higher capacity, better rate behavior and cycling stability than C@MoS_2 microspheres. The reasons can be attributed to the

DOI: 10.1021/acsami.5b06002
ACS Appl. Mater. Interfaces 2015, 7, 22927–22934

interconnected nanospherical morphology and the internal hierarchical construction of these nanospheres with expanded MoS_2/carbon interlayer spacing. Facile synthesis and good performance of the hierarchical nanospherical C@MoS_2 as well as its good compatibility with the traditional manufacturing technology of Li-ion batteries render it a promising functional material for application in energy storage and conversion systems.

AUTHOR INFORMATION

Corresponding Authors

*E-mail: qtqu@suda.edu.cn. (Q.Q.)
*E-mail: hhzheng@suda.edu.cn. (H.Z.)

Notes

The authors declare no competing financial interest.

ACKNOWLEDGMENTS

This work was supported by National Natural Science Foundation of China (NSFC Nos. 21203133, 21301124, 21473120, and 51272168) and The Natural Science Foundation of Jiangsu Province (BK2012186).

REFERENCES

(1) Stephenson, T.; Li, Z.; Olsen, B.; Mitlin, D. Lithium Ion Battery Applications of Molybdenum Disulfide (MoS_2) Nanocomposites. *Energy Environ. Sci.* **2014**, *7*, 209−231.

(2) Zhou, F.; Xin, S.; Liang, H. W.; Song, L. T.; Yu, S. H. Carbon Nanofibers Decorated with Molybdenum Disulfide Nanosheets: Synergistic Lithium Storage and Enhanced Electrochemical Performance. *Angew. Chem., Int. Ed.* **2014**, *53*, 11552−11556.

(3) Yu, X.-Y.; Hu, H.; Wang, Y.; Chen, H.; Lou, X. W. Ultrathin MoS_2 Nanosheets Supported on N-doped Carbon Nanoboxes with Enhanced Lithium Storage and Electrocatalytic Properties. *Angew. Chem., Int. Ed.* **2015**, *54*, 7395−7398.

(4) Zhou, J.; Qin, J.; Zhang, X.; Shi, C.; Liu, E.; Li, J.; Zhao, N.; He, C. 2D Space-Confined Synthesis of Few-Layer MoS_2 Anchored on Carbon Nanosheet for Lithium-Ion Battery Anode. *ACS Nano* **2015**, *9*, 3837−3848.

(5) Choi, S. H.; Ko, Y. N.; Lee, J.-K.; Kang, Y. C. 3D MoS_2−Graphene Microspheres Consisting of Multiple Nanospheres with Superior Sodium Ion Storage Properties. *Adv. Funct. Mater.* **2015**, *25*, 1780−1788.

(6) Wang, J. Z.; Lu, L.; Lotya, M.; Coleman, J. N.; Chou, S. L.; Liu, H. K.; Minett, A. I.; Chen, J. Development of MoS_2-CNT Composite Thin Film from Layered MoS_2 for Lithium Batteries. *Adv. Energy Mater.* **2013**, *3*, 798−805.

(7) Su, D.; Dou, S.; Wang, G. Ultrathin MoS_2 Nanosheets as Anode Materials for Sodium-Ion Batteries with Superior Performance. *Adv. Energy Mater.* **2015**, *5*, 1401205.

(8) Zhu, C.; Mu, X.; van Aken, P. A.; Maier, J.; Yu, Y. Fast Li Storage in MoS_2-Graphene-Carbon Nanotube Nanocomposites: Advantageous Functional Integration of 0D, 1D, and 2D Nanostructures. *Adv. Energy Mater.* **2015**, *5*, 1401170.

(9) Yang, T.; Chen, Y. J.; Qu, B. H.; Mei, L.; Lei, D. N.; Zhang, H. N.; Li, Q. H.; Wang, T. H. Construction Of 3D Flower-Like MoS_2 Spheres with Nanosheets as Anode Materials for High-Performance Lithium Ion Batteries. *Electrochim. Acta* **2014**, *115*, 165−169.

(10) Kong, D. B.; He, H. Y.; Song, Q.; Wang, B.; Lv, W.; Yang, Q. H.; Zhi, L. J. Rational Design of MoS_2@Graphene Nanocables: Towards High Performance Electrode Materials for Lithium Ion Batteries. *Energy Environ. Sci.* **2014**, *7*, 3320−3325.

(11) Jeong, J.-M.; Lee, K. G.; Chang, S.-J.; Kim, J. W.; Han, Y.-K.; Lee, S. J.; Choi, B. G. Ultrathin Sandwich-Like MoS_2@N-Doped Carbon Nanosheets For Anodes Of Lithium Ion Batteries. *Nanoscale* **2015**, *7*, 324−329.

(12) Lu, Y.; Yao, X.; Yin, J.; Peng, G.; Cui, P.; Xu, X. MoS_2 Nanoflowers Consisting of Nanosheets with a Controllable Interlayer Distance as High-Performance Lithium Ion Battery Anodes. *RSC Adv.* **2015**, *5*, 7938−7943.

(13) Shi, Y. M.; Wang, Y.; Wong, J. I.; Tan, A. Y. S.; Hsu, C. L.; Li, L. J.; Lu, Y. C.; Yang, H. Y. Self-assembly of Hierarchical MoS_x/CNT Nanocomposites ($2 < X < 3$): Towards High Performance Anode Materials for Lithium Ion Batteries. *Sci. Rep.* **2013**, *3*, 2169.

(14) Lu, C. X.; Liu, W. W.; Li, H.; Tay, B. K. A Binder-Free CNT Network-MoS_2 Composite as a High Performance Anode Material in Lithium Ion Batteries. *Chem. Commun.* **2014**, *50*, 3338−3340.

(15) Ma, L.; Ye, J. B.; Chen, W. X.; Chen, D. Y.; Yang Lee, J. Gemini Surfactant Assisted Hydrothermal Synthesis of Nanotile-Like MoS_2/Graphene Hybrid with Enhanced Lithium Storage Performance. *Nano Energy* **2014**, *10*, 144−152.

(16) Huang, G. C.; Chen, T.; Chen, W. X.; Wang, Z.; Chang, K.; Ma, L.; Huang, F. H.; Chen, D. Y.; Lee, J. Y. Graphene-Like MoS_2/Graphene Composites: Cationic Surfactant-Assisted Hydrothermal Synthesis and Electrochemical Reversible Storage of Lithium. *Small* **2013**, *9*, 3693−3703.

(17) Cao, X. H.; Shi, Y. M.; Shi, W. H.; Rui, X. H.; Yan, Q. Y.; Kong, J.; Zhang, H. Preparation of MoS_2-Coated Three-Dimensional Graphene Networks for High-Performance Anode Material in Lithium-Ion Batteries. *Small* **2013**, *9*, 3433−3438.

(18) Chang, K.; Chen, W. L-Cysteine-Assisted Synthesis of Layered MoS_2/Graphene Composites with Excellent Electrochemical Performances for Lithium Ion Batteries. *ACS Nano* **2011**, *5*, 4720−4728.

(19) Xie, X. Q.; Ao, Z. M.; Su, D. W.; Zhang, J. Q.; Wang, G. X. MoS_2/Graphene Composite Anodes with Enhanced Performance for Sodium-Ion Batteries: The Role of the Two-Dimensional Heterointerface. *Adv. Funct. Mater.* **2015**, *25*, 1393−1403.

(20) Liu, Y.; Zhao, Y.; Jiao, L.; Chen, J. A Graphene-Like MoS_2/Graphene Nanocomposite As A Highperformance Anode For Lithium Ion Batteries. *J. Mater. Chem. A* **2014**, *2*, 13109−13115.

(21) Wang, R. H.; Xu, C. H.; Sun, J.; Liu, Y. Q.; Gao, L.; Yao, H. L.; Lin, C. C. Heat-Induced Formation of Porous and Free-Standing MoS_2/GS Hybrid Electrodes for Binder-Free and Ultralong-Life Lithium Ion Batteries. *Nano Energy* **2014**, *8*, 183−195.

(22) Zhang, L.; Lou, X. W. Hierarchical MoS_2 Shells Supported on Carbon Spheres for Highly Reversible Lithium Storage. *Chem. - Eur. J.* **2014**, *20*, 5219−5223.

(23) Xu, X.; Fan, Z. Y.; Yu, X. Y.; Ding, S. J.; Yu, D. M.; Lou, X. W. A Nanosheets-on-Channel Architecture Constructed from MoS_2 and CMK-3 for High-Capacity and Long-Cycle-Life Lithium Storage. *Adv. Energy Mater.* **2014**, *4*, 1400902.

(24) Jiang, H.; Ren, D.; Wang, H.; Hu, Y.; Guo, S.; Yuan, H.; Hu, P.; Zhang, L.; Li, C. 2D Monolayer MoS_2−Carbon Interoverlapped Superstructure: Engineering Ideal Atomic Interface for Lithium Ion Storage. *Adv. Mater.* **2015**, *27*, 3687.

(25) Wan, Z. M.; Shao, J.; Yun, J. J.; Zheng, H. Y.; Gao, T.; Shen, M.; Qu, Q. T.; Zheng, H. H. Core-Shell Structure of Hierarchical Quasi-Hollow MoS_2 Microspheres Encapsulated Porous Carbon as Stable Anode for Li-Ion Batteries. *Small* **2014**, *10*, 4975−4981.

(26) Qiu, W. D.; Xia, J.; He, S. X.; Xu, H. J.; Zhong, H. M.; Chen, L. P. Facile Synthesis of Hollow MoS_2 Microspheres/Amorphous Carbon Composites and Their Lithium Storage Properties. *Electrochim. Acta* **2014**, *117*, 145−152.

(27) Sun, P.; Zhang, W.; Hu, X.; Yuan, L.; Huang, Y. Synthesis Of Hierarchical MoS_2 and its Electrochemical Performance as an Anode Material for Lithium-ion Batteries. *J. Mater. Chem. A* **2014**, *2*, 3498−3504.

(28) Xu, M.; Yi, F.; Niu, Y.; Xie, J.; Hou, J.; Liu, S.; Hu, W.; Li, Y.; Li, C. M. Solvent-Mediated Directionally Self-Assembling MoS_2 Nanosheets into a Novel Worm-Like Structure and its Application in Sodium Batteries. *J. Mater. Chem. A* **2015**, *3*, 9932−9937.

(29) Wang, M.; Li, G. D.; Xu, H. Y.; Qian, Y. T.; Yang, J. Enhanced Lithium Storage Performances of Hierarchical Hollow MoS_2 Nanoparticles Assembled from Nanosheets. *ACS Appl. Mater. Interfaces* **2013**, *5*, 1003−1008.

DOI: 10.1021/acsami.5b06002
ACS Appl. Mater. Interfaces 2015, 7, 22927−22934

(30) Ding, S. J.; Zhang, D. Y.; Chen, J. S.; Lou, X. W. Facile Synthesis of Hierarchical MoS_2 Microspheres Composed of Few-Layered Nanosheets and their Lithium Storage Properties. *Nanoscale* **2012**, *4*, 95−98.
(31) Zhang, L.; Wu, H. B.; Yan, Y.; Wang, X.; Lou, X. W. Hierarchical MoS_2 Microboxes Constructed by Nanosheets with Enhanced Electrochemical Properties for Lithium Storage and Water Splitting. *Energy Environ. Sci.* **2014**, *7*, 3302−3306.
(32) Sun, T.; King, H. E. Aggregation Behavior in the Semidilute Poly(N-Vinyl-2-Pyrrolidone)/Water System. *Macromolecules* **1996**, *29*, 3175−3181.
(33) Qu, Q.; Fu, L.; Zhan, X.; Samuelis, D.; Maier, J.; Li, L.; Tian, S.; Li, Z.; Wu, Y. Porous $LiMn_2O_4$ as Cathode Material with High Power and Excellent Cycling for Aqueous Rechargeable Lithium Batteries. *Energy Environ. Sci.* **2011**, *4*, 3985−3990.
(34) Wei Seh, Z.; Li, W. Y.; Cha, J. J.; Zheng, G. Y.; Yang, Y.; McDowell, M. T.; Hsu, P. C.; Cui, Y. Sulphur-TiO_2 Yolk-Shell Nanoarchitecture with Internal Void Space for Long-Cycle Lithium-Sulphur Batteries. *Nat. Commun.* **2013**, *4*, 1331.
(35) Zheng, F.; He, M.; Yang, Y.; Chen, Q. Nano Electrochemical Reactors Of Fe_2O_3 Nanoparticles Embedded in Shells of Nitrogen-Doped Hollow Carbon Spheres as High-Performance Anodes for Lithium-Ion Batteries. *Nanoscale* **2015**, *7*, 3410−3417.
(36) Xiao, J.; Wang, X.; Yang, X.-Q.; Xun, S.; Liu, G.; Koech, P. K.; Liu, J.; Lemmon, J. P. Electrochemically Induced High Capacity Displacement Reaction of PEO/MoS_2/Graphene Nanocomposites with Lithium. *Adv. Funct. Mater.* **2011**, *21*, 2840−2846.
(37) Dominko, R.; Arčon, D.; Mrzel, A.; Zorko, A.; Cevc, P.; Venturini, P.; Gaberscek, M.; Remskar, M.; Mihailovic, D. Dichalcogenide Nanotube Electrodes for Li-Ion Batteries. *Adv. Mater.* **2002**, *14*, 1531−1534.
(38) Liu, Y.; Jiao, L.; Wu, Q.; Du, J.; Zhao, Y.; Si, Y.; Wang, Y.; Yuan, H. Sandwich-structured Graphene-like MoS_2/C Microspheres for Rechargeable Mg Batteries. *J. Mater. Chem. A* **2013**, *1*, 5822−5826.
(39) Wang, J. J.; Luo, C.; Gao, T.; Langrock, A.; Mignerey, A. C.; Wang, C. S. An Advanced MoS_2/Carbon Anode for High-Performance Sodium-Ion Batteries. *Small* **2015**, *11*, 473−481.

DOI: 10.1021/acsami.5b06002
ACS Appl. Mater. Interfaces 2015, 7, 22927−22934